Parallel colour-opponent pathways to primary visual cortex

Soumya Chatterjee & Edward M. Callaway

Systems Neurobiology Laboratories, The Salk Institute for Biological Studies, 10010 North Torrey Pines Road, La Jolla, California 92037, USA, and Neuroscience Program, University of California 92093, San Diego, California, USA

The trichromatic primate retina parses the colour content of a visual scene into 'red/green' and 'blue/yellow' representations[1–2]. Cortical circuits must combine the information encoded in these colour-opponent signals to reconstruct the full range of perceived colours[3]. Red/green and blue/yellow inputs are relayed by the lateral geniculate nucleus (LGN) of thalamus to primary visual cortex (V1), so understanding how cortical circuits transform these signals requires understanding how LGN inputs to V1 are organized. Here we report direct recordings from LGN afferent axons in muscimol-inactivated V1. We found that blue/yellow afferents terminated exclusively in superficial cortical layers 3B and 4A, whereas red/green afferents were encountered only in deeper cortex, in lower layer 4C. We also describe a distinct cortical target for 'blue-OFF' cells, whose afferents terminated in layer 4A and seemed patchy in organization. The more common 'blue-ON' afferents were found in 4A as well as lower layer 2/3. Chromatic information is thus conveyed to V1 by parallel, anatomically segregated colour-opponent systems, to be combined at a later stage of the colour circuit.

The retina constructs colour-opponency from cones sensitive to long (L), middle (M) and short (S) wavelengths by superimposing excitatory (ON) and inhibitory (OFF) signals from different parts of the visible spectrum[1,2,4]. Midget ganglion cells compare photon catches between L and M cones, creating a red/green opponent axis. Small and large bistratified cells relay ON signals from S cones and OFF signals from L+M cones (blue-ON receptive fields), giving rise to a blue/yellow colour axis. And an achromatic channel is established by parasol cells, which sum their cone contributions.

These ganglion cells send their outputs to the LGN, which in turn projects at least three parallel pathways (magno-, parvo- and koniocellular) to V1. Neurons in magno layers carry the achromatic signal from parasol cells to layer 4Cα of V1, whereas parvo neurons relay the red/green input of midget cells to layer 4Cβ[5–10]. Cells in koniocellular zones, which may receive blue-ON input from small bistratified cells[7,11–13], project to superficial layers of V1[14]. However, konio cells do not respect laminar borders strictly, and are often found in neighbouring parvo and magno layers. The spatial overlap of neuronal populations has confounded attempts to uniquely correlate receptive field properties with cell types and their cortical projections. Thus, it is not known whether blue-ON cells recorded in parvo layers[3,15–18] are parvo cells projecting to layer 4Cβ or displaced konio cells terminating in superficial V1. It is also unclear whether konio cells carry any red/green opponency to superficial layers. Finally, some konio or parvo cells may have blue-OFF receptive fields[3,17,19], but their cortical targets have not been identified.

We examined the functional organization of colour-opponent input to V1 by silencing cortical neurons with the $GABA_A$ agonist muscimol, which allowed us to record directly from LGN afferent terminals in various depths of cortex. Most afferents could be unambiguously classified into four groups: blue-ON, blue-OFF, red/green or achromatic, each with its own visual response signature. Cone-isolating, drifting sinusoidal gratings at optimal temporal and spatial frequencies were used to determine the contributions of different cone types. The cell shown in Fig. 1a was robustly driven by S-cone-isolating gratings as well as L+M gratings, with responses shown in peristimulus time histograms (PSTHs, lower part of Fig. 1a). Furthermore, the first harmonic phases of the S and L+M responses were almost 180° apart (anti-phase); that is, the peak of the S-cone-isolating stimulus influenced the cell's firing with the same sign (ON or OFF) as the trough of the L+M grating, indicating blue/yellow colour-opponency.

We recovered the signs of these cone inputs from cone-isolating reverse-correlation experiments. Spike-triggered averages (STAs) were obtained by showing a long sequence of randomly chosen, rapidly presented stimuli (sine-wave gratings of various orientations, spatial frequencies and phases, drawn from the two-dimensional Hartley basis set[20]), and calculating the average stimulus that elicited a spike. The time course of the S-cone-isolating STA for a group of pixels representing the cell's receptive field centre is shown in the upper part of Fig. 1a (blue trace). The horizontal axis represents the 250-ms epoch before each spike, and the vertical axis is the STA cone contrast, where +1 and −1 are the maximum

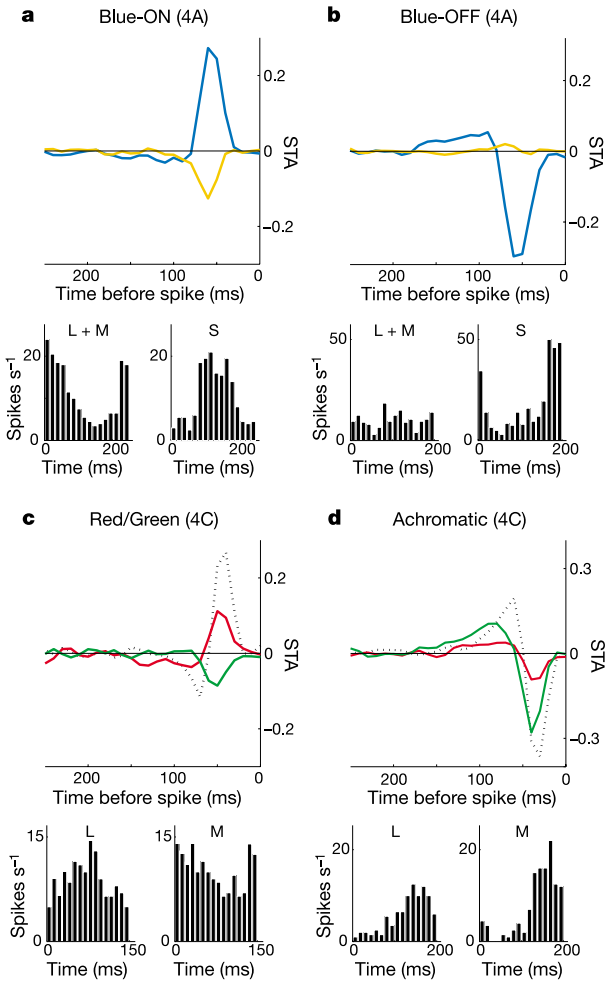

Figure 1 LGN afferents recorded in muscimol-inactivated V1 were classified into four distinct groups on the basis of cone contributions. STAs for L (M, S, L+M, L+M+S) cone-isolating stimuli are shown in red (green, blue, yellow, dotted black). **a**, Characterization of a blue-ON afferent, encountered in layer 4A of V1. Shown (lower part of the panel) are the cell's responses to cone-isolating, drifting gratings, binned over multiple grating cycles into PSTHs with horizontal axes equal to the temporal period of the stimulus. The upper part of the panel summarizes data from reverse-correlation experiments using cone-isolating Hartley stimuli. **b**, A blue-OFF afferent recorded in layer 4A, with same conventions as in **a**. **c**, A red/green afferent recording, from layer 4C. **d**, An achromatic afferent encountered in layer 4C.

and minimum achievable cone excitation for each stimulus. The upward deflection of the trace indicates an ON response to S-cone activation, whereas the downward transient seen with L+M cone-isolating stimuli (yellow trace) reveals OFF input from L and M cones, establishing this as a blue-ON cell with cone contributions very similar to those of blue-ON small bistratified cells of the retina[21]. Blue-OFF cells were characterized in the same manner (Fig. 1b). Cone-isolating gratings drove a vigorous S response and extremely weak L+M response (which was often the case for blue-OFF cells that we encountered). STAs computed for this cell confirm that the S-cone signal was OFF.

Distinguishing blue-ON and blue-OFF from red/green afferents was straightforward, as the latter were marked by L/M opponency (Fig. 1c) and little or no S-cone input. All chromatic units, in turn, were distinct from achromatic afferents (Fig. 1d), which exhibited no opponency between cone types. (See Supplementary Fig. S1 for population data related to classification.)

To examine how chromatic inputs to V1 were organized, we reconstructed the locations of recording sites in relation to cortical layers for individual electrode penetrations, following electrolytic lesions and histology. Figure 2a shows a tangential penetration in silenced V1 traversing roughly 2.5 mm of superficial cortex from first to last recorded unit. With the electrode skirting the boundary between layer 2/3 and 4A, we found multiple clusters of blue-ON afferents (while crossing four ocular dominance transitions). Finally going through layer 4A near the end of the penetration, we encountered a cluster of blue-OFF afferents. Out of 14 penetrations with recovered lesions, 5 contained both blue-ON and blue-OFF recordings (Fig. 2a–e). Each showed this surprising input pattern, with blue-ON afferents in lower 2/3 + 4A terminating above blue-OFF. As an additional five penetrations had blue-ON with no blue-OFF (example in Fig. 2i), and given the greater number of blue-ON afferents encountered (comprising 78% of S-cone-dominated afferents in our sample), it is likely that blue-ON geniculate projections to V1 have a more extensive coverage of superficial cortex. Blue-OFF cells, on the other hand, seem to terminate in sparse patches, segregated by depth from blue-ON.

The overall laminar organization of inputs to V1 is exemplified by the penetration shown in Fig. 2e. We encountered different afferent classes in a highly specific laminar order: blue-ON → lower 2/3+4A, blue-OFF → 4A, achromatic → upper 4C, and red/green → lower 4C. This pattern was conserved across our data set. Axonal projections of magno and parvo neurons to 4Cα and 4Cβ, respectively, are consistent with achromatic input to upper and red/green

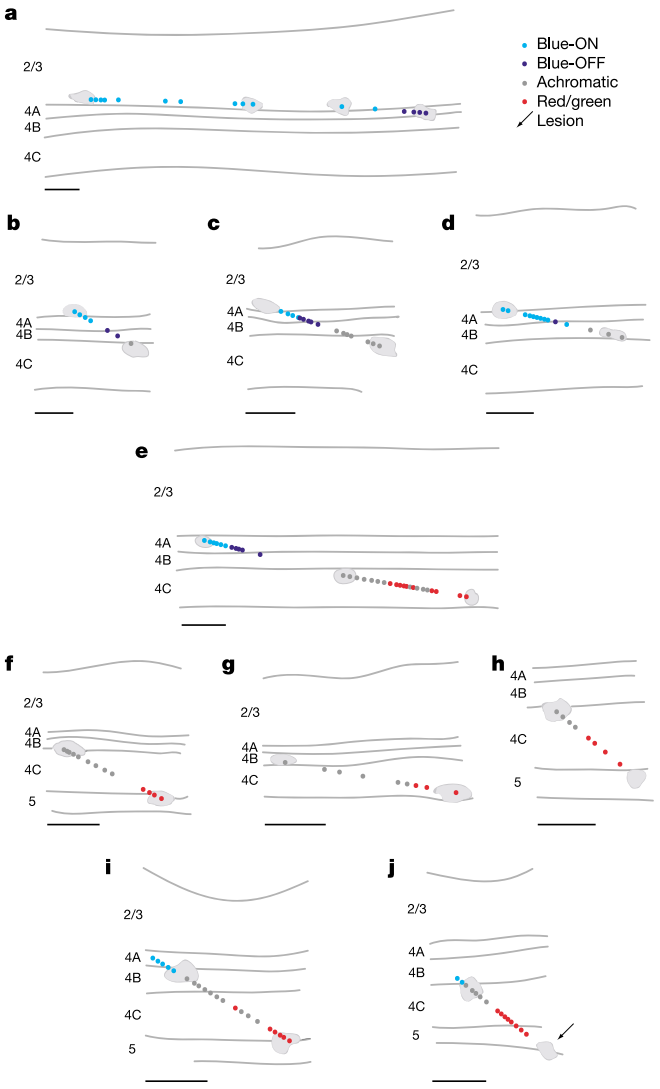

Figure 2 Reconstructions of tangential electrode penetrations in muscimol-inactivated V1. Coloured markers (light blue, dark blue, red and grey) indicate the locations of individual LGN afferent recordings and their colour opponencies (blue-ON, blue-OFF, red/green and achromatic, respectively). **a**–**e**, The five penetrations in which both blue-ON and blue-OFF afferents were encountered show a functional organization of S-cone-dominated afferents based on depth, with blue-ON inputs terminating above blue-OFF in almost all cases. **e**–**j**, Achromatic and red/green inputs were restricted to upper and lower 4C, respectively. The direction of each penetration is aligned from left to right, and lesions used for electrode track reconstructions are shown as grey patches, as indicated by the arrow in **j**. Scale bar, 250 μm.

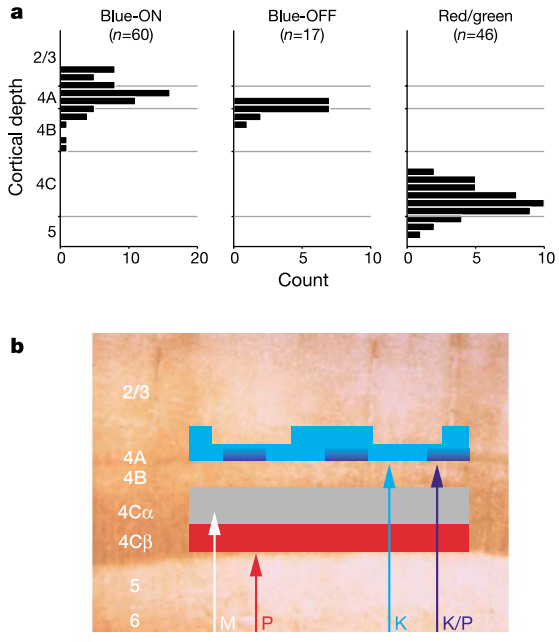

Figure 3 Laminar organization of colour-opponent afferents. **a**, Histograms show the laminar distribution of all blue-ON, blue-OFF and red/green afferents recorded in V1. Blue-OFF afferents were restricted to the lower part of the blue-ON range, and both were segregated from red/green input with no overlap. **b**, Diagram describing hypothesized relationships between physiology of colour inputs and anatomical projections. Achromatic and red/green afferents to layer 4C almost certainly arise from magno (M) and parvo (P) contributions to 4Cα and 4Cβ, respectively. Blue-ON inputs to layers 4A and 2/3 are most probably koniocellular. Blue-OFF afferents could be koniocellular (K), but there is also evidence supporting a parvo projection to 4A, raising the possibility that a separate blue-OFF parvo substream bypasses its usual target of 4Cβ to project solely to 4A.

to lower 4C (Fig. 2e–j). We analysed 221 afferent recordings (60 blue-ON, 17 blue-OFF, 46 red/green, and 98 achromatic), and the laminar distribution of colour-opponent inputs shows complete segregation of blue/yellow and red/green axes (Fig. 3a). Crucially, no red/green afferents were encountered in supragranular layers, and no blue/yellow input was found in 4C.

Columnar organization of blue/yellow and red/green input is not likely. Such organization predicts some population heterogeneity at a given laminar depth as the electrode tangentially cuts across putative columns over multiple penetrations. Because no mixing of blue/yellow and red/green afferents was seen in any layer after recording from a total ~4.3 mm of lower 2/3 + 4A and ~5.4 mm of 4C (measurements post-histology, so normal tissue shrinkage of 20–40% underestimates coverage), our observations strongly imply a laminar organization instead. There is heterogeneity between blue-ON and -OFF in layer 4A, but if blue-OFF terminations are patchy, they are not columnar in the classical sense because they do not extend above or below 4A. They may, however, still be related to some overall columnar architecture of V1 (for example, blobs). Also, different classes of red/green cells (all the permutations between centre/surround and ON/OFF L- and M-cone contributions) were treated as one group in this study, because we saw no clear sublaminar or columnar organization of these classes.

Because extracellular recordings are subject to considerable sampling bias, it is possible that red/green afferents do project to upper layers and we simply did not encounter them. The same argument applies to blue/yellow input to 4C, as well as to the apparent patchiness of blue-OFF input to 4A. Also, despite focused attempts, we could not record from upper layer 2/3 or 1, where some afferents from konio layers are thought to project[14]. Perhaps the upper layer 2/3 inputs are numerically weaker or have fewer terminal branches than those to lower layer 2/3 and 4A. Given that not one of 77 LGN afferents recorded in superficial cortex was red/green, however, it seems reasonable that if such a projection exists, it is either very sparse or consists of terminal arbors whose morphologies preclude successful recording.

We have shown that LGN afferents terminating in lower 2/3 and 4A are functionally distinct from those projecting to layer 4C, consistent with anatomical studies suggesting that afferents terminating in either location do not terminate in both[10]. Interpreted within the context of parallel anatomical projections from magno, parvo and konio LGN to V1, it seems that red/green, blue/yellow and achromatic inputs are carried by different systems, and are partitioned with these pathways to different input layers of cortex (Fig. 3b). Our observations strongly suggest that koniocellular neurons, the small cells retrogradely labelled from superficial cortex and scattered in and around konio layers, are the carriers of blue-ON and perhaps blue-OFF input to superficial layers in the macaque monkey. We found no afferents in superficial layers relaying red/green input, a role that seems to belong to the parvocellular projection to 4Cβ. This bears on a recent hypothesis[22] that states that the parvo system is used for spatial processing only (as it is the pathway of highest visual acuity), whereas the konio system is the dedicated pathway for colour information, carrying both red/green and blue/yellow signals to a putative colour circuit in superficial cortex. Unless a completely separate population projects to upper 2/3, the segregation of red/green afferents to 4Cβ makes this scenario unlikely.

It is important to note that ambiguities in the definitions and properties of LGN parvo or konio cells prevent us from definitively identifying all blue/yellow neurons as konio. Ideally, konio cells might be defined as those that project to superficial layers (4A and above) and that express the neurochemical markers calbindin and αCaM kinase. But there is evidence suggesting that at least some afferents terminating in layer 4A do not express these proteins[14]. Thus, if defined by their superficial projections, the blue-ON and -OFF cells that we encountered are konio. If defined by their neurochemical signature, some of the 4A input could be parvo. The highly stereotyped response properties of blue-ON inputs to layers 4A and 2/3 suggest that these inputs arise from a single population, most probably koniocellular. Blue-OFF afferents were never found above 4A and are a separate population functionally. Retrograde tracer injections encroaching on layer 4A (but not more superficially) tend to label cells in the parvo layers of LGN that do not express αCaM kinase or calbindin, possibly implicating a separate parvo pathway to 4A as the carrier of blue-OFF signals[14]. Retinal anatomy shows that S cones contact OFF midget bipolars[23], which in turn contact midget ganglion cells[24], which may be the provenance of this putative subsystem.

A final distinction awaits further work, but it seems clear that the blue-OFF pathway is anatomically and functionally distinct from both blue-ON and red/green systems, and that blue/yellow and red/green opponent systems include separate pathways terminating in distinct laminar zones in V1. □

Methods

Animal preparation and data collection

Seven juvenile macaque monkeys were used in this study (three *Macaca mulatta*, four *Macaca radiata*). Each animal was anaesthetized (sufentanil citrate) and paralysed (pancuronium bromide), and dexamethasone was given to reduce brain swelling. Eyes were dilated, protected with gas-permeable contact lenses, and refracted with external lenses. We made a large (~8 × 5 mm) craniotomy over the parafoveal representation in striate cortex, reflected dura, and placed a ~7 × 5 mm section of Gelfoam onto the pial surface, leaving a small gap between skull and Gelfoam to tangentially introduce an electrode. The craniotomy was sealed with bone wax and warm agar, with a tube running through to the Gelfoam to administer muscimol (50 mM in 0.9% saline, 0.1–0.2 ml h^{-1}). Muscimol perfusion inactivated all V1 neurons under the Gelfoam patch, through layer 6.

Geniculate afferent spikes were recorded with sharp, low-impedance electrodes (1–2 MΩ at 1 kHz) and sorted with custom software (PEP, D. Ringach). After encountering the first afferent 'hash' (usually lower layer 2/3 or 4A), we advanced 20–40 μm between recordings, isolating the largest spikes present. These were most probably summed across terminal branches of single axons and not fibres of passage, because layers 4B and 5 (through which axons to superficial layers must pass) generally had no isolatable spikes and very little background activity. The large patch of inactivated cortex precludes our recording from axons of intrinsic horizontal connections. Slight shifts in receptive field position between consecutive recording sites, as well as the known convergence of many geniculate axons to any given point in the input layers of V1[25], argue against our consistently recording from the same axon at different sites along a penetration. See ref. 26 for a more complete discussion of the muscimol method of afferent recording. All procedures were approved by the Salk Institute Animal Care and Use Committee.

Histology

Small electrolytic lesions (3.5 μA for 3.5 s, electrode tip negative) were made in cortex to guide the reconstruction of electrode tracks. After transcardial perfusion, the brain was blocked, sunk in 30% sucrose, and sectioned (50 μm) on a freezing microtome. Tissue was stained for cytochrome oxidase to define layers. Owing to the length of the experiment (4–5 days) and the elimination of cortical activity, blobs could not be reliably recovered.

Visual stimuli and display calibration

Visual stimuli were generated on a Silicon Graphics O_2 computer using custom software (PEP, D. Ringach) and shown on a calibrated CRT display run at 100 Hz refresh rate. The three monitor guns were linearized with respect to frame buffer value, and their additivity verified. The monitor was placed 100 cm from the animal.

Cone-isolating stimuli were constructed from human cone fundamentals[27] and the measured spectral power distributions of monitor phosphors[28]. The peak and trough of each stimulus modulated about a fixed grey background (each linearized gun at half-maximal intensity, mean luminance of ~28 cd m^{-2}, CIE colour coordinates $x = 0.29$, $y = 0.27$). Each stimulus (L, M, S, L+M and L+M+S) was presented at the maximum cone contrast achievable by our monitor, which for L (M, S) was 0.23 (0.28, 0.90). The L+M stimulus consisted of 0.55 cone contrast for L summed with 0.64 for M.

Circular patches of drifting sinusoidal gratings (radius ~1–2°) were shown at the cell's optimal temporal and spatial frequencies. Stimuli isolating different cone directions were presented in random order for 4 s each, with a blank trial inserted after every third grating. We typically averaged over 3–4 such trials per cell. In reverse-correlation experiments, Hartley stimuli[20] were randomly drawn and presented at every other screen refresh (every 20 ms), for a duration of ~15–20 min per cone direction.

Our calibration methods were checked by constructing cone-isolating stimuli for three sets of glass filters (L, Oriel 59500+Schott BG-40; M, Schott VG-9; S, Oriel 59814+Oriel 59080) whose transmissions approximated the spectral absorptions of L, M and S cones[29]. We measured the power of these cone-isolating stimuli through each filter set with a photodiode, and found that each stimulus isolated its intended model cone at least 30 times better than the other two model cones. In addition, the multiple physiological controls in a previous study by the authors[30] (including controls for L/M/rod intrusion

into S-cone responses using a very bright yellow adapting light, as well as tests for chromatic aberration by varying the spatial frequency of cone-isolating stimuli from near full-field to optimal) apply to the present study, because apparatus, set-up and calibration methods were identical.

Received 16 June; accepted 15 October 2003; doi:10.1038/nature02163.

1. Lennie, P. & D'Zmura, M. Mechanisms of color vision. *Crit. Rev. Neurobiol.* **3,** 333–400 (1988).
2. Dacey, D. M. Parallel pathways for spectral coding in primate retina. *Annu. Rev. Neurosci.* **23,** 743–775 (2000).
3. De Valois, R. L., Cottaris, N. P., Elfar, S. D., Mahon, L. E. & Wilson, J. A. Some transformations of color information from lateral geniculate nucleus to striate cortex. *Proc. Natl Acad. Sci. USA* **97,** 4997–5002 (2000).
4. Dacey, D. M., Peterson, B. B., Robinson, F. R. & Gamlin, P. D. Fireworks in the primate retina. *In vitro* photodynamics reveals diverse LGN-projecting ganglion cell types. *Neuron* **37,** 15–27 (2003).
5. Leventhal, A. G., Rodieck, R. W. & Dreher, B. Retinal ganglion cell classes in the Old World monkey: Morphology and central projections. *Science* **213,** 1139–1142 (1981).
6. Michael, C. R. Retinal afferent arborization patterns, dendritic field orientations, and the segregation of function in the lateral geniculate nucleus of the monkey. *Proc. Natl Acad. Sci. USA* **85,** 4914–4918 (1988).
7. Conley, M. & Fitzpatrick, D. Morphology of retinogeniculate axons in the macaque. *Vis. Neurosci.* **2,** 287–296 (1989).
8. Hubel, D. & Wiesel, T. Laminar and columnar distribution of geniculo-cortical fibers in the macaque monkey. *J. Comp. Neurol.* **146,** 421–450 (1972).
9. Hendrickson, A. E., Wilson, J. R. & Ogren, M. P. The neuroanatomical organization of pathways between the dorsal lateral geniculate nucleus and visual cortex in Old World and New World primates. *J. Comp. Neurol.* **182,** 123–136 (1978).
10. Blasdel, G. G. & Lund, J. S. Termination of afferent axons in macaque striate cortex. *J. Neurosci.* **3,** 1389–1413 (1983).
11. Rodieck, R. W. & Watanabe, M. Survey of the morphology of macaque retinal ganglion cells that project to the pretectum, superior colliculus, and parvicellular laminae of the lateral geniculate nucleus. *J. Comp. Neurol.* **338,** 289–303 (1993).
12. Martin, P. R., White, A. J., Goodchild, A. K., Wilder, H. D. & Sefton, A. E. Evidence that blue-on cells are part of the third geniculocortical pathway in primates. *Eur. J. Neurosci.* **9,** 1536–1541 (1997).
13. Hendry, S. H. & Reid, R. C. The koniocellular pathway in primate vision. *Annu. Rev. Neurosci.* **23,** 127–153 (2000).
14. Hendry, S. H. & Yoshioka, T. A neurochemically distinct third channel in the macaque dorsal lateral geniculate nucleus. *Science* **264,** 575–577 (1994).
15. Wiesel, T. N. & Hubel, D. H. Spatial and chromatic interactions in the lateral geniculate body of the rhesus monkey. *J. Neurophysiol.* **29,** 1115–1156 (1966).
16. Schiller, P. H. & Malpeli, J. G. Functional specificity of lateral geniculate nucleus laminae of the rhesus monkey. *J. Neurophysiol.* **41,** 788–797 (1978).
17. Derrington, A. M., Krauskopf, J. & Lennie, P. Chromatic mechanisms in lateral geniculate nucleus of macaque. *J. Physiol. (Lond.)* **357,** 241–265 (1984).
18. Reid, R. C. & Shapley, R. M. Space and time maps of cone photoreceptor signals in macaque lateral geniculate nucleus. *J. Neurosci.* **22,** 6158–6175 (2002).
19. Valberg, A., Lee, B. B. & Tigwell, D. A. Neurones with strong inhibitory S-cone inputs in the macaque lateral geniculate nucleus. *Vision Res.* **26,** 1061–1064 (1986).
20. Ringach, D. L., Sapiro, G. & Shapley, R. A subspace reverse-correlation technique for the study of visual neurons. *Vision Res.* **37,** 2455–2464 (1997).
21. Dacey, D. M. & Lee, B. B. The 'blue-on' opponent pathway in primate retina originates from a distinct bistratified ganglion cell type. *Nature* **367,** 731–735 (1994).
22. Calkins, D. J. & Sterling, P. Evidence that circuits for spatial and color vision segregate at the first retinal synapse. *Neuron* **24,** 313–321 (1999).
23. Ahmad, K. M., Klug, K., Herr, S., Sterling, P. & Schein, S. Cell density ratios in a foveal patch in macaque retina. *Vis. Neurosci.* **20,** 189–209 (2003).
24. Klug, K., Herr, S., Ngo, I. T., Sterling, P. & Schein, S. J. Macaque retina contains an S-cone OFF midget pathway. *J. Neurosci.* **23,** 9881–9887 (2003).
25. Blasdel, G. G. & Fitzpatrick, D. Physiological organization of layer 4 in macaque striate cortex. *J. Neurosci.* **4,** 880–895 (1984).
26. Chapman, B., Zahs, K. R. & Stryker, M. P. Relation of cortical cell orientation selectivity to alignment of receptive fields of the geniculocortical afferents that arborize within a single orientation column in ferret visual cortex. *J. Neurosci.* **11,** 1347–1358 (1991).
27. Stockman, A., MacLeod, D. I. & Johnson, N. E. Spectral sensitivities of the human cones. *J. Opt. Soc. Am. A* **10,** 2491–2521 (1993).
28. Wandell, B. A. *Foundations of Vision* 413–421 (Sinauer, Sunderland, MA, 1995).
29. Chichilnisky, E. J. & Baylor, D. A. Receptive-field microstructure of blue-yellow ganglion cells in primate retina. *Nature Neurosci.* **2,** 889–893 (1999).
30. Chatterjee, S. & Callaway, E. M. S cone contributions to the magnocellular visual pathway in macaque monkey. *Neuron* **35,** 1135–1146 (2002).

Supplementary Information accompanies the paper on **www.nature.com/nature**.

Acknowledgements We thank D. Ringach for providing software used for visual stimulation, spike sorting, and some data analysis; E. J. Chichilnisky for help with stimulus calibration and design; and E. J. Chichilnisky and G. Horwitz for a critical reading of the manuscript. We also thank S. Tye for surgical assistance.

Competing interests statement The authors declare that they have no competing financial interests.

Correspondence and requests for materials should be addressed to S.C. (sochatte@ucsd.edu).

Development and maintenance of B and T lymphocytes requires antiapoptotic MCL-1

Joseph T. Opferman, Anthony Letai, Caroline Beard, Mia D. Sorcinelli, Christy C. Ong & Stanley J. Korsmeyer

Howard Hughes Medical Institute, Dana Farber Cancer Institute, Department of Pathology and Medicine, Harvard Medical School, Boston, Massachusetts 02115, USA

Regulated apoptosis is essential for both the development and the subsequent maintenance of the immune system[1,2]. Interleukins, including IL-2, IL-4, IL-7 and IL-15, heavily influence lymphocyte survival during the vulnerable stages of VDJ rearrangement and later in ensuring cellular homeostasis, but the genes specifically responsible for the development and maintenance of lymphocytes have not been identified[3–8]. The antiapoptotic protein MCL-1 is an attractive candidate, as it is highly regulated[9], appears to enhance short-term survival[10] and functions at an apical step in genotoxic deaths[11]. However, *Mcl-1* deficiency results in peri-implantation lethality[12]. Here we show that mice conditional for *Mcl-1* display a profound reduction in B and T lymphocytes when MCL-1 is removed. Deletion of *Mcl-1* during early lymphocyte differentiation increased apoptosis and arrested the development at pro-B-cell and double-negative T-cell stages. Induced deletion of *Mcl-1* in peripheral B- and T-cell populations resulted in their rapid loss. Moreover, IL-7 both induced and required MCL-1 to mediate lymphocyte survival. Thus, MCL-1, which selectively inhibits the proapoptotic protein BIM, is essential both early in lymphoid development and later on in the maintenance of mature lymphocytes.

The proapoptotic 'BH3-only' members of the BCL-2 family respond to selective death signals and trigger activation of the 'multidomain' death effectors BAX and BAK, which constitute an obligate gateway to the intrinsic death pathway. Conversely, antiapoptotic BCL-2 members have an important role in binding and sequestering BH3-only molecules, thus preventing activation of BAX and BAK[13,14]. BH3 domains can be subdivided into those that 'activate' (for example, BID and BIM) by inducing oligomerization of BAX and BAK, or those that 'sensitize' (for example, BAD and BIK) by occupying the pocket of antiapoptotic family members[15]. Individual BCL-2 family members have specific roles. Haematopoiesis is initially normal in *Bcl-2*-deficient animals, but over time lymphocytes are vulnerable to apoptosis, particularly following activation stimuli[16]. *Bcl-X_L*-deficient lymphocytes show that it is critical for the survival of $CD4^+CD8^+$ double-positive (DP) thymocytes, but not for mature T cells[17,18].

We generated a conditional *Mcl-1* allele by targeting *loxP* sites upstream of the ATG start codon and between exons 1 and 2 (Fig. 1a). This *Mcl-1*$^{flox(f)}$ allele was transmitted through the germ line, and matings of *Mcl-1*$^{f/wt}$ mice yielded viable *Mcl-1*$^{f/f}$ offspring at the expected mendelian frequency (Supplementary Fig. 1a–d). Both *Mcl-1*$^{f/wt}$ and *Mcl-1*$^{f/f}$ cells express levels of MCL-1 protein comparable to wild-type (wt) cells (Fig. 1b and Supplementary Fig. 3a). We also generated an *Mcl-1*^{null} allele in which portions of *Mcl-1* exons 1 and 2 were replaced with an internal ribosome entry site allowing the expression of a neomycin–β-galactosidase fusion protein (Fig. 1a). *Mcl-1*$^{f/null}$ murine embryonic fibroblasts (MEFs) after Cre-mediated deletion, *Mcl-1*$^{deleted/null}$ (Δ/*null*), lack detectable MCL-1 protein (Fig. 1b).

To restrict deletion of the *Mcl-1*^{f} allele to T-cell development, we introduced the lymphocyte-specific protein tyrosine kinase–Cre